# EFFICACY AND COMPATIBILITY OF AN INNOVATIVE IN-HOUSE DYNAMIC LIVER HEPATOCELLULAR CARCINOMA PHANTOM FOR MAGNETIC RESONANCE IMAGING APPLICATIONS

**MONTASER W M SAIED AHMAD**

**UNIVERSITI SAINS MALAYSIA**

**2021**

# EFFICACY AND COMPATIBILITY OF AN INNOVATIVE IN-HOUSE DYNAMIC LIVER HEPATOCELLULAR CARCINOMA PHANTOM FOR MAGNETIC RESONANCE IMAGING APPLICATIONS

**by**

**MONTASER W M SAIED AHMAD**

**Thesis submitted in fulfilment of the requirements**
**for the degree of**
**Doctor of Philosophy**

**January 2021**

**DEDICATION**

*This work is dedicated to*

**PROPHET MUHAMMAD BIN ABDOLLAH BIN ABDULMUTALIB, HIS FAMILY AND COMPANIONS**

## ACKNOWLEDGEMENT

"In the name of Allah, the most Gracious, the most merciful"

My gratitude and praise to ALLAH, the Almighty, the greatest of all, on whom ultimately, we depend for sustenance and guidance. I would like to thank Almighty Allah for giving me opportunity, determination and strength to do my research. His continuous grace and mercy was with me throughout my life and ever more during the tenure of my research.

I would like to express my sincere gratitude to my advisor Dr. Nursakinah Suardi for the continuous support of my PhD study and related research, for his patience, motivation, and immense knowledge. Thank you for supervising my thesis work and for supporting and encouraging me along the way, and for enthusiasm and inspiration which was always there when I needed it. Her guidance helped me in all the time of research and writing of this thesis. I could not have imagined having a better advisor and mentor for my PhD study.

Besides my advisor, I would like to thank the rest of my thesis committee: Prof. Dato' Dr. Ahmad Shukri Mustapa Kamal, Dr. Nik Noor Ashikin Nik Ab Razak, and Dr. Mohammad I Hjouj, for their insightful comments and encouragement, but also for the hard question which incented me to widen my research from various perspectives.

My sincere thanks also go to Dr. Ammar A. Oglat, Dr. Mohammed al-Haj, and Dr. Osama Makhamrah, who provided me an opportunity to join their team as intern, and who gave access to the laboratory and research facilities. Without they precious support it would not be possible to conduct this research. Many thanks to my parents and my family for their support and encouragement over the last year.

MUNTASER S. AHMAD, 2020

## TABLE OF CONTENTS

## LIST OF TABLES

**Page**

## LIST OF FIGURES

**Page**

## LIST OF ABBREVIATIONS

| | |
|---|---|
| AASLD | American Association for the Study of Liver Diseases |
| ADC | Apparent diffusion coefficient |
| AFP | α-fetoprotein |
| ASTM | American Society for Testing Materials |
| BPCAs | Blood Pool Agents |
| BZK | Benzalkonium Chloride |
| C.S | Compression strength |
| CA | Contrast Agent |
| CNR | Contrast to Noise Ratio |
| CT | Computed Tomography |
| CV | Coefficient Variation |
| DCE | Direct Contrast Enhancement |
| DCE | Dynamic Contrast-Enhanced |
| DP | Delayed Phase |
| DWI | Diffusion Weighting Image |
| EASL-EORTC | European Association for the Study of the Liver–European Organisation for Research and Treatment of Cancer |
| ECCM | Extracellular Contrast Media-Enhancement |
| ECFAs | Extracellular Fluid Agents |
| EOB | Ethoxybenzyl |
| FDG PET/CT | Fluorodeoxyglucose Positron Emission Tomography Hybrid with Computed Tomography |
| FDS | Frequency Domain Spectroscopy |
| FID | Free Induction Decay |
| FLASH | Fast Low-Angle Shot |
| FOV | Field of View |

| | |
|---|---|
| FSE | Fast Spin-Echo |
| FTIR | Fourier Transform Infrared Spectroscopy |
| GBCAs | Extracellular Gadolinium-Based Contrast Agents |
| GBHCAs | Gadolinium-Based Hepatobiliary Contrast Agents |
| HAP | Late Hepatic Arterial Phase |
| HASTE | Half-Fourier Acquisition Single-Shot Turbo Spin-Echo |
| HBP | Hepatobiliary Phase |
| HBV | Hepatitis B |
| HCC | Hepatocellular Carcinoma |
| HCV | Hepatitis C-virus |
| HEC | Hydroxyethyl Cellulose |
| HGF | Hepatocyte Growth Factor |
| HSC | Hepatic Stellate Cells |
| HSI | Hyperspectral Imaging |
| IGF | Insulin Growth Factor |
| IP | In-phase Image |
| IR-SE | Inversion Recovery Spin Echo |
| KVO | Keep Vein Open |
| LHCC | Large Hepatocellular Carcinoma |
| LITT | Laser-Induced Interstitial Thermotherapy |
| MHz | Megahertz |
| MIR | Mid-Infrared Spectroscopy |
| MRI | Magnetic Resonance Imaging |
| MVI | Microvascular Invasion |
| NAFLD | Non-Alcoholic Fatty Liver Disease |
| NIRS | Near-Infrared Spectroscopy |

| | |
|---|---|
| NIST | National Institute of Standards and Technology |
| NMV | Net Magnetization Vector |
| OP | Out of Phase |
| Pa | Pascal |
| PAA | Polyacrylamide |
| PD | Proton Density |
| PDC | polarization and depolarization current |
| PDGF | Platelet-derived Growth Factor |
| PET | Positron Emission Tomography |
| ppm | Parts Per Million |
| PVA | Polyvinyl Alcohol |
| PVC | Polyvinyl Chloride |
| PVP | Porto venous Phase |
| QRM | Quality Assurance in Radiology and Medicine |
| RF | Radio-Frequency |
| RFA | Radiofrequency Ablation |
| ROI | Region of Interest |
| RTV | Room-Temperature-Vulcanizing |
| sHCC | small Hepatocellular Carcinoma |
| SNR | Signal to Noise Ratio |
| SPECT | Single Photon Emission Computed Tomography |
| SPGR | Spoiled Gradient Recalled Echo |
| TAC | Time-Attenuation Curves |
| TE | Echoing Time |
| TGF-β | Transforming Growth Factor Beta |
| TI | Inversion Time |
| TMM | Tissue- Mimicking Materials |

| | |
|---|---|
| TR | Repetition Time |
| TSE | Turbo Spin-Echo |
| US | Ultrasound |
| VIBE | Volumetric Interpolated Breath-hold Examination |
| VST | Vibrational Spectroscopic Techniques |

## LIST OF SYMBOLS

| | |
|---|---|
| A | Atomic mass |
| Z | Atomic number |
| k | Boltzmann's constant |
| $^{13}C$ | Carbon atom |
| $d\varphi$ | Changing magnetic flux in a single loop |
| dt | Changing time |
| σ | Conductivity |
| $CuSO_4$ | Copper Sulfate |
| ° | Degree |
| ε | Emf |
| $B_0$ | External magnetic field |
| $\theta$ | Flip angle. |
| $^{19}F$ | Fluorine |
| $M_0$ | Full longitudinal magnetization |
| $GdCl_3$ | Gadolinium (III) Chloride |
| $g$ | Gram |
| γ | Gyro magnetic ratio |
| $^{1}H$ | Hydrogen atom |
| J | Joules |
| K | Kelvin |
| $\omega_0$ | Larmor frequency |
| $T_1$ | Longitudinal relaxation time |
| $MnCl_2$ | Manganese (II) Chloride |
| $NiCl_2$ | Nickel (II) Chloride |
| $^{15}N$ | Nitrogen atom |

| | |
|---|---|
| $^{17}O$ | Oxygen atom |
| psi | Pound per square inch |
| k | Scaling factor |
| sec | Second |
| S/m | Siemens per meter |
| $^{23}Na$ | Sodium atom |
| $N^-$ | Spins-down |
| $N^+$ | Spins-up |
| $T_2^*$ | $T_2$*-weighted imaging |
| T | Temperature |
| $Mxy_t$ | Transverse magnetization |
| $T_2$ | Transverse relaxation time |
| V | Volts |
| wt% | Weight percentage |

**KEBERKESANAN DAN KESESUAIAN INOVATIF DALAMAN DINAMIK FANTOM HATI KARSINOMA HEPATOSELULAR UNTUK KEGUNAAN DI DALAM PENGIMEJAN MAGNETIK RESONAN**

## ABSTRAK

Kaedah radiologi yang berbeza digunakan untuk mendiagnosis pelbagai penyakit, termasuk kanser. Pengimejan magnetik resonans (MRI) adalah salah satu kaedah yang digunakan untuk memperlihatkan tisu manusia dalam bentuk 3D. Parameter yang berbeza digunakan dalam visualisasi tisu lembut menghasilkan kualiti gambar yang berbeza. Untuk tujuan ini, fantom digunakan untuk memeriksa kualiti gambar yang dihasilkan oleh peranti dan juga untuk membezakan di antara tisu normal dan patologi. Sifat fantom harus setara dengan sifat tubuh manusia. Beberapa kajian sebelumnya menggunakan polimer untuk mensimulasikan sifat setara tubuh manusia, seperti karsinoma hati dan hepatoselular (HCC). Walau bagaimanapun, kajian yang telah mengkaji kestabilan sifat fantom yang diwakili HCC dalam bentuk dinamiknya adalah terhad. Oleh itu, kajian ini bertujuan untuk mengkaji kestabilan sifat fantom dalam jangka masa enam minggu di samping mensimulasikan HCC secara dinamik. Dalam kajian ini, parenkima hati disimulasikan menggunakan tiga bahan yang berbeza dengan kepekatan yang berbeza: gelatin (dengan kepekatan 2.5wt%, 4 wt%, dan 5 wt%); sampel gelatin-agar (gelatin dengan kepekatan 2.5 wt%, 4 wt%, dan 5 wt%) dicampurkan dengan kepekatan agar adalah malar (1.5wt%) dalam semua sampel, dan akhirnya, sampel agarosa-lilin (agarosa dengan kepekatan 2.5 wt%, 4.5 wt%, dan 6 wt%) dicampurkan dengan kepekatan lilin adalah malar pada 2.6 wt%. Pengukuran bagi sifat yang berbeza untuk semua sembilan sampel diukur dalam jangka masa enam minggu iaitu: sifat kimia yang diwakili oleh jenis ikatan antara komponen, sifat

mekanik yang diwakili oleh ketumpatan dan kekuatan mampatan, sifat elektrik yang diwakili oleh kekonduksian, dan ciri pengimejan MR yang ditunjukkan oleh $T_1$dan masa rehat $T_2$. Sampel HCC dibuat dalam berbagai ukuran (2 cm, 1 cm, dan 0.5 cm) untuk mengetahui ukuran terkecil yang dapat dikesan menggunakan peranti MR. Hasil kajian menunjukkan sampel agarosa-lilin dengan kepekatan 2.5wt% adalah sampel ketumpatan yang paling stabil di antara sampel lain (nilai P, 0.648), sedangkan sampel gelatin dengan kepekatan 2.5wt% adalah nilai ketumpatan terdekat kepada ketumpatan hati manusia dengan perbezaan mencapai 1.92%. Perubahan kekuatan mampatan meningkat dengan peningkatan kepekatan gelatin pada sampel agar-agar dan gelatin-agar, dan juga meningkat dengan peningkatan kepekatan agarosa pada sampel agarosa-lilin. Walau bagaimanapun, sampel agarose-lilin dengan kepekatan 2.5wt% adalah nilai kekuatan mampatan terdekat berbanding dengan hati manusia. Sampel agarose-lilin adalah nilai terdekat dengan kekonduksian hati manusia. Sampel terdekat hati manusia pada masa relaksasi $T_1$ dan $T_2$ ditunjukkan dalam sampel lilin agarose terutama dalam kepekatan agarose 2.5% wt dengan perbezaan 2.4% berbanding tahap rujukan untuk gambar berat $T_1$ dan 3 kali lebih tinggi daripada tahap rujukan untuk Gambar berat $T_2$. Walau bagaimanapun, perubahan terbesar pada masa relaksasi adalah pada minggu kelima semua sampel terutama pada sampel agarose-lilin (nilai P, 0,047). Perbezaan masa relaksasi disebabkan oleh kitaran pengosongan air dan penyerapannya ke dalam bekasnya. Hasilnya juga menunjukkan corak khas HCC. Ukuran HCC terendah yang dapat diukur dalam MRI adalah 1.0 cm menggunakan gegelung badan dan 0.5 cm menggunakan gegelung kepala. Kesimpulannya, hati manusia disimulasikan menggunakan TMM termasuk gelatin, agar-agar, dan agarosa lilin. Sementara HCC disimulasikan menggunakan poliuretana dan gliserin. Parameter

HASTE, FLASH, dan Dixon-VIBE yang sesuai juga diperoleh untuk mengesan HCC dengan MRI.

**EFFICACY AND COMPATIBILITY OF HEPATOCELLULAR-MIMICKING IN LIVER DYNAMIC PHANTOM FOR USE IN MAGNETIC RESONANCE APPLICATIONS**

## ABSTRACT

Different radiology modalities are used to diagnose various diseases, including cancer. Magnetic resonance imaging (MRI) is one of non-invasive modalities used to visualize human tissue in 3D technique. Different parameters used in the visualization of the soft tissues results with different image quality. For this purpose, phantom is used to check the image quality produced by the device and also to distinguish between normal and pathological tissues. The properties of the phantom should be similar to those of the human body. Several previous studies used polymers to simulate the similar properties of the human body, like liver and hepatocellular carcinoma (HCC). However, limited studies have studied the stability of the phantom properties represented HCC in their dynamic form. Therefore, the present study aims to investigate the phantom properties stability over a period of six weeks in addition to simulate the HCC in a dynamic way. In this study, the liver parenchyma was simulated using three different substances with different concentrations: gelatin (with concentration of 2.5wt%, 4 wt%, and 5 wt%); gelatin-agar samples (gelatin with concentration of 2.5wt%, 4 wt%, and 5 wt%) is mixed with constant agar concentration (1.5wt%) in all gelatin-agar samples, and finally, agarose-wax samples (agarose with concentration of 2.5 wt%, 4.5 wt%, and 6 wt%) is mixed with a constant wax concentration 2.6 wt%. Different properties for all nine samples were measured over period of six weeks which are: chemical properties represented by the type of bonds

between the components, mechanical properties represented by density and compressive strength, electrical properties represented by conductivity, and MR imaging characteristics represented in $T_1$ and $T_2$ relaxation times. HCC samples were fabricated using polyurethane and glycerol in different sizes (0.5 cm, 1.0 cm, and 2.0 cm) to know the smallest size that could be detected using MR device. The results of the study showed the agarose-wax sample with concentration of 2.5wt% was the most stable sample in density among other samples (P-value, 0.648), while the gelatin sample with concentration of 2.5wt% was the closest density value to the human liver density with difference reached to 1.92%. The changing of compression strength increases with increasing gelatin concentration in both gelatin and gelatin-agar samples, and it also increases with increasing agarose concentration in agarose-wax samples. However, the agarose-wax sample with concentration of 2.5wt% was the closest compression strength value compared to the human liver. Also, the agarose-wax samples were the closest value to the human liver conductivity. The closest samples of the human liver on $T_1$ and $T_2$ relaxation times were represented in the agarose-wax samples especially in agarose concentration of 2.5%wt with differences 2.4% comparing to reference level for $T_1$-weight image and 3 times higher than reference level for $T_2$-weight image. However, the largest changes in relaxation times were in the fifth week of all samples especially in agarose-wax samples (P-value, 0.047). The difference in relaxation times is due to the water evacuation cycles and its absorption into its containers. The results also showed the typical pattern of HCC. The lowest size of HCC could be measured in MRI was 1.0 cm using body coil and 0.5 cm using head coil. In conclusion, the human liver was simulated using TMMs including gelatin, gelatin agar, and agarose wax. While HCC was simulated using polyurethane

and glycerin. Also, the appropriate HASTE, FLASH, and Dixon-VIBE-derived parameters were obtained for the detection of HCC with MRI.

# CHAPTER 1

# INTRODUCTION

## 1.1 Background of the Study

Cancer is considered as the most common diseases in the world and threatening human life at a very high rate annually. Hepatocellular carcinoma (HCC) is one of the most common cancer in the human body which originates in the liver and most HCC cases are detected at the later stage (Heimbach *et al*., 2018; Galle *et al*., 2018). Early detection of HCC increases the treatment efficiency by 60% compared to the delayed detection. Several techniques are used to detect HCC; α-fetoprotein (AFP); ultrasound (US); computed tomography (CT); magnetic resonance imaging (MRI); and fluorodeoxyglucose positron emission tomography hybrid with computed tomography (FDG PET/CT) (Ahmad *et al*., 2019).

Researchers and medical practitioners need a tool that can be used in experiments before human trials. The ideal characteristics of tool are easy to be used without any complications, continuously available, and cost-effective. Phantoms are used in many medical applications such as developing medical techniques, improving image quality in different medical imaging techniques, helping surgeons to improve their job performance, and helping to detect various diseases (Rethy *et al*., 2018; Surry *et al*., 2004). For MRI application, there are many characteristics in terms of chemical, mechanical, electrical and imaging properties should be in the phantom to simulate the various organs within the human body. Liver MRI phantoms have been used for various purposes including the development of new pulse sequences; calibration MRI equipment; surgery action training for liver surgery; and needle guided puncture of lesions (Yoshida *et al*., 2004; Rethy *et al*., 2018).

$T_1$ and $T_2$ weighted images sequences are considered as an essential sequence in MRI applications for diagnosing of different diseases in the liver such as liver cirrhosis (Petitclerc *et al*., 2017), fatty liver (Middleton *et al*., 2018), hepatic iron overload (Sheth *et al*., 2019) and HCC (Ahmad *et al*., 2020). The quantitative sequences in MRI are utilized for diagnosis, staging, and monitoring of HCC. Nowadays, many clinical trials use an MRI system to assess the HCC treatment such as selective internal radiation therapy, sorafenib, radiofrequency ablation, and others (Heimbach *et al*., 2018; Galle *et al*., 2018). Different MRI variables should be understood to enable proper HCC assessment including fat suppression, image distortion caused by geometric distortion, and signal variations using body coil. Therefore, standard references level or phantoms are used to evaluate these variables.

Phantom can be used in MRI, where it is in one of two forms, either aqueous solutions or polymer gels. Aqueous solutions such as manganese (II) chloride ($MnCl_2$), copper sulfate ($CuSO_4$), gadolinium (III) chloride ($GdCl_{3)}$, and nickel (II) chloride ($NiCl_2$) are used for testing MRI equipment due to its stability for a long time with homogeneous relaxation time. However, the aqueous phantoms do not mimic human tissue well and it needs a container to maintain form. In the previous studies, the polymer gel phantoms using different types of material which have been used to fabricate the liver phantom for MRI imaging such as polyacrylamide (PAA) (Groch *et al*., 1991), carrageenan gel (Yoshimura *et al*., 2003;Kato *et al*., 2005), agar gel (Bucciolini *et al*., 1989), agarose gel (Hopper *et al*., 2006;Shevchenko *et al*., 2010), gelatin (Chmarra *et al*., 2013), polyurethane (Rethy *et al*., 2018), polyvinyl alcohol (PVA) (Surry *et al*., 2004), polysaccharide gels TX-150 (Groch *et al*., 1991) and TX-151 (Mazzara *et al*., 1996). In addition, some of these substances have been used to simulate HCC such as agarose-glycerol (Shevchenko *et al*., 2010) and polyurethane

material (Rethy *et al*., 2018). Gelatin and agar powders have been used in many previous studies to simulate different organs within the body such as head and neck (Kandadai *et al*., 2012a; Richardson *et al*., 2015), breast (Sutcliffe *et al*., 2013; Madsen *et al*., 2003), skin (Chao *et al*., 2013; Lacik *et al*., 2016), spine ( Li *et al*., 2011; Gallo *et al*., 2015), and thyroid gland (Abraham, 2014). These materials can also be used to simulate the human liver (Opik *et al*., 2012; Chmarra *et al*., 2013).

An ideal MRI liver phantom should fulfill characteristics which include: design for quantitatively evaluating standard proton spin relaxation time ($T_1$, $T_2$); support relaxation times in a uniform way with the ability to change times $T_1$ and $T_2$ independently; capacity to be shaped into forms similar to those of human organs; compatibility with body coil; easy preparation; no deterioration of quality over a long period; and ability to simulate the heterogeneous distribution between disease samples and normal liver parenchyma (Yoshimura *et al*., 2003; Ahmad *et al*., 2019). Many studies have succeeded in simulating human liver with HCC phantom. However, limited phantoms fabrication of dynamic pattern of HCC is available.

## 1.2 Problem Statement

HCC is considered as primary carcinoma in the liver, and the third vital carcinoma in the world after lung and colorectal cancer. It was described as the fifth and seventh most common cancer in men and women, respectively (Galle *et al*., 2018). Non-invasive imaging is an important method to detect stages of HCC. The basic concept of HCC development is to detect strange vascular perturbation, which occurs through hepatic carcinogenesis. The HCC detection is based on contrast enhancement in diagnostic modalities like CT and MRI. There are three phases enhancement to visualize the lesions: late hepatic arterial phase (HAP), portovenous phase (PVP), and delayed phase (DP) (Ahmad *et al*., 2019). The HCC has a typical hallmark of contrast

enhancement because the HCC receives nutrients directly from the hepatic artery while the parenchymal liver cells derive oxygen and nutrients via the portal vein. Thus, the HCC has shown as a hyper-vascularity in the HAP, while in the PVP it shows less hyperintensity due to contrast washout and at the DP hypo-intensity (complete wash) appears. These features known as classic feature (Heimbach *et al*., 2018).

Early detection of HCC would reduce the risk of developing carcinogenesis. At this stage, HCC would be demonstrated as hypo-vascular because the arterial feeding has not fully developed. Lesions of less than 2 cm must be detected because delaying diagnosis decreases the treatment efficiency or increases the chance of tumor recurrences. The HCC nodules with diameters of less than 1 cm has not been demonstrated yet.

MRI is one of the most advanced techniques in 3D imaging of the internal organs in the human body. Unlike conventional radiology instruments like CT which used ionising radiation, MRI and US do not use ionising radiation to produce images. Therefore, there are minimal side effects of these techniques representing in the thermal effect on the body. MRI and US techniques are considered non-invasive imaging helps doctors in detecting diseases, because they have a great ability to differentiate between normal and pathological tissues.

The sensitivity of MRI and US diagnostic performance for HCC depends on tumor size. The MRI has a 62% sensitivity for detecting small lesions less than 2 cm versus 95% for detection lesions more than 2 cm (Galle *et al*., 2018). While, the sensitivity of US to detect HCC in early stage is reported as 25.6-47% (Bruix *et al*., 2016; Choi *et al*., 2016; Khalili, 2019) versus 93% for detecting advanced HCC stage (Heimbach *et al*., 2018). However, the sensitivity of CT scan for detecting HCC is the

lowest compared to the US and MRI, where early-stage HCC detection was reported at 45% versus 92% for the detection of advanced-stage HCC (Heimbach *et al*., 2018). It is considered suboptimal comparing with MRI (Kim *et al*., 2016). MRI with the contrast agent improves the detection of HCC which is usually missed with US. Therefore, the current study relied on using MRI technique instead of US.

Several previous studies have succeeded in simulating human liver parenchyma with HCC phantom and applied it under MRI using several materials such as gelatin, agar, and agarose. These studies relied mainly on the distinction between normal parenchyma tissue and HCC within the phantom based on the difference in signal intensity (Shevchenko *et al*., 2010; Chmarra *et al*., 2013; Rethy *et al*., 2018). However, limited studies are available for fabrication the dynamic phantom of HCC in detecting stages of this cancer. Given this scenario, the current research problem lies in the development of a dynamic phantom representing the liver parenchyma and HCC and also helping to find a method to distinguish the stages of HCC cancer in application under MRI. Fabrication of dynamic phantom is important because early detection of HCC is one of the priorities that medical practitioners are looking for to help provide efficient and effective treatment for this cancer and early diagnosis of HCC.

There are several issues need to be considered when using dynamic phantom which are; the phantom should be in a container that allows the transfer of contrast material from the arteries to the veins through the study samples; the substance of the sample should appear like the disease to be simulated (HCC), the sample should allow the interaction with contrast material and successfully ejected out without changing the structure; the possibility of changing the pathologic samples (HCC) without affecting the whole organ structure (liver parenchyma); and finally, the phantom

should allow the pumping process and disposing of the contrast material using automatic injector and suction device.

## 1.3 Research Objective

The current research aims to develop a phantom that mimics the human liver. In addition to simulate HCC in its physical properties and apply the phantom under MRI. The phantom should be suitable for teaching, training and equipment development purposes in the field of MRI with real-time imaging. Therefore, the specific objectives of this study are:

1. To characterise and assess the best tissue-mimicking materials (TMMs) in terms of chemical, mechanical, electrical and imaging properties, and its stability over the period of time.
2. To fabricate dynamic liver-HCC phantom with different TMMs for MRI applications.
3. To propose optimum MRI scanning parameters and sequences that can be utilised to assess and detect the HCC behavior.

## 1.4 Scope of the Research

This research is focused on characteristics of TMMs used in fabrication of liver parenchyma and HCC samples. The challenge in this research is represented in dynamic phantom application. Furthermore, preparation of a suitable liver TMMs using in liver parenchyma and examine its MRI features by applying $T_1$ and $T_2$ parameters.

Liver TMMs were made with different materials mainly are; 2.6 wt % of dry weight Hydroxyethyl cellulose (HEC) powder, 0.2 wt % of Benzalkonium chloride (BZK), 3.2 wt % of propanediol, and distilled water with different weight percentage

of gelatin, agar, wax, and agarose. All of phantoms are characterized in terms of chemical, mechanical, electrical, and MRI properties. The stability of phantom properties is examined over period of six weeks. Also, the effect of time interval on signal intensity of $T_1$ and $T_2$ weighted imaging was measured.

## 1.5 Significant of the study

The importance of the current study lies in simulating HCC dynamically by fabricating a liver phantom that mimics the human liver and then simulating HCC from materials that mimic this cancer inside the liver. Subsequently, the idea of a dynamic phantom form (this form allows the MRI contrast agent to be applied through the use of four phases: the pre-contrast phase; arterial phase; portovenous phase; and delay phase) was developed and applied under MRI. To help in early detection of HCC by changing the parameters used in imaging the abdomen routinely in order to know the best parameters that should be used to detect this cancer in an early stage.

## 1.6 Outline of Thesis

This thesis is arranged into five chapters. Chapter one explains the study background, motivation and problem statement, research objectives, study scope and thesis organization. The first chapter focused on the main point of the research. Chapter two describes the comprehensive literature review and theory for the study including anatomy and physiology of the liver, MRI (signal generation, relaxation and reconstruction), imaging properties ($T_1$ and $T_2$ signal intensities), MRI acquisition protocols (Half-Fourier Acquisition Single-Shot Turbo Spin-Echo, Fast Low-Angle Shot, and Dixon sequences), MRI Phantoms characterizations (chemical, mechanical, and electrical), and live phantom (including parenchyma, HCC samples, and dynamic phantom). Chapter three explains the instruments (apparatus), materials used in this research, and the methodology including experimental preparation of liver

parenchyma, experimental and scanning setups, MRI protocols, and data acquisition. Chapter four displays the analysis of the result and discussion of the data obtained in this study. Chapter five presents the conclusion and recommendations for the research.

# CHAPTER 2

# THEORY AND LITERATURE REVIEW

## 2.1 Introduction

Many previous studies have included MRI applications such as investigations of body organs elasticity, quality assurance of treatment, and guidance for surgical purposes. In fact, these applications have increased significantly in recent times. The existence of methods like phantoms help the development of these applications without need to deal with the human body directly. The phantom helped medical practitioners and researchers to develop many MRI applications. Many studies focused on the phantom properties to make the applications more realistic.

## 2.2 Anatomy and Physiology of Liver

Liver is the largest organ in the human body located in the right part of the body, and it is covered the lower rib from 7-11$^{th}$ ribs. The liver consists of four asymmetric lobes; right and left lobes in the front surface separated by falciform ligament, and quadrate and caudate lobes located in the posterior surface (see Figure 2.1) (Zündorf, 2007). The gallbladder is located under the liver and the stomach is located on the left. The weight of liver is between 1.2 and 1.6 kg in healthy adults, which weighs 2.5-3% of the total body weight (Demetris *et al*., 2016).

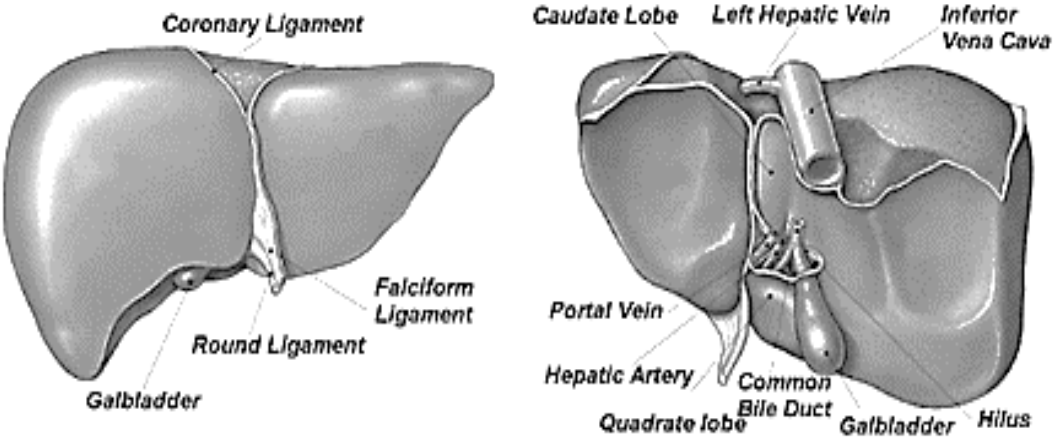


Figure 2. 1: Anterior and posterior views of the Liver (Zündorf, 2007).

The liver is supplied with blood by hepatic artery that connects directly to the aorta which is coming from heart, as well as the portal vein that supplies the liver with nutrients which comes from stomach, spleen, and intestines. The hepatic artery supplies the liver only 25% of the blood and the rest 75% supplies from portal vein. The deoxygenated blood leaves liver through hepatic vein which is connected to the inferior vena cava.

The liver has more than 100 functions, due to that liver is considered as one of the major organs in the body. Some of these functions are bile secretion, nutrients metabolism, bilirubin metabolism, sort of mineral, amino-acid synthetization, protein synthetization, Insulin Growth Factor (IGF) synthetization, thromboprotein production, carbohydrate metabolism, lipid metabolism, cholesterol phospholipids synthetization, plasma protein synthetization, urea production, and others (Marieb & Keller, 2017; Moriyama *et al*., 2000).

## 2.3 Magnetic Resonance Imaging

MRI is one of the most diagnostic techniques used in the medical field to depict anatomy organs in human body. MRI is based on the nuclear atom movements within the body. According to Faraday's Law, a charged particle orbiting around itself creates a small magnetic field. The idea of MRI depends on the odd number protons especially hydrogen atom (H), which revolves around its axis to create a spin. MRI based on H atom in term of signal intensity more than other atoms because the H atom in human body are the most abundant element. In addition to that the hydrogen proton has the largest gyro magnetic ratio (γ)among other atoms (Goyen, 2006).

MRI is safer than other techniques because it does not use ionising radiation to produce an anatomical image, unlike conventional X-ray, CT and even positron emission tomography (PET) or single photon emission computed tomography (SPECT). Instead of that, MRI uses a strong external magnetic field and radio-wave to produce the images. Moreover, MRI can produce the best contrast differentiation in soft tissue, produce a 3D volumetric image, produce any orientation images including axial, coronal and sagittal; and is capable of using at different applications like MR spectroscopy (Barker *et al*., 2009).

The contrast of MR imaging depends on both intrinsic tissue properties and extrinsic properties. The intrinsic properties include tissue density, the different relaxation time of the tissue, and the hydrogen concentration in the tissue. The extrinsic properties are represented for any outside parameter such as repetition time (TR), echoing time (TE), flip angle, and inversion time (TI). The differences in these parameters influence the reconstructed image ( Bushong , 2015). The MRI imaging processes are presented in three steps: signal generation, detection, and reconstruction.

### 2.3.1 Signal Generation

The basic of producing MRI image depends on atoms motion. Indeed, there are three different motions found in the atom; electron spinning around own axis; electron spinning around the nucleus within orbits; and nucleus spinning around own axis. Figure 2.2 shows these three types of motions.

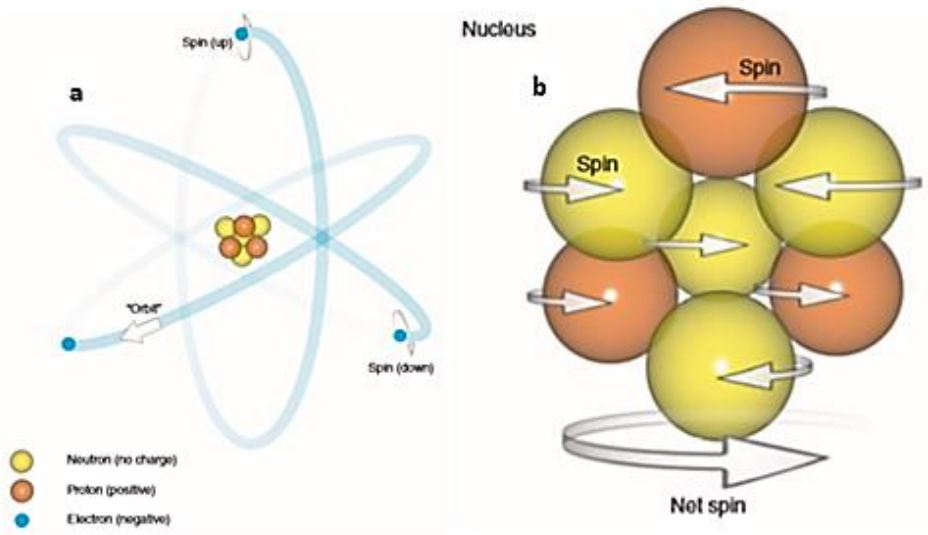


Figure 2. 2: The atom motions; (a): electron spinning around own axis and orbiting around nucleus; (b): nucleus spinning around own axis ( Mamourian *et al*., 2011).

The atom motions are different in various biological tissues. Also, the spinning motion depends on the atomic mass (A) and atomic number (Z). If the A equals to Z, the nucleus has not spinning because half of spinning are in the same direction and the other half in the different direction. Thus, the net magnetization vector (NMV) reaches to zero. However, if the A is different from Z, then there are nucleus spinning around its own axis, and this spinning is called angular momentum.

Scientist Michael Faraday in 1833 discovered the law of electromagnetic induction, which states that any charged object orbiting itself generates a magnetic field (Alexander, 2010). The magnetic field indicates by magnetic moment (magnitude) and magnetic direction (vector). The NMV is the sum of total magnetic moment which presents at the same vector (Reeve *et al*., 2018). The most important MRI active nuclei in the human body are; hydrogen ($^{1}$H); carbon ($^{13}$C); nitrogen ($^{15}$N); oxygen ($^{17}$O); fluorine ($^{19}$F); and sodium ($^{23}$Na).

The protium (hydrogen isotopes with one proton only) is the most famous MR-active nucleus is the most abundant nuclei and gives the largest magnetic moment in the human body. In the natural state, the nuclei are randomly orientated and the NMV equals to zero. However, when the strong external magnetic field ($B_0$) applied, the hydrogen magnetic moments orientate with this magnetic field. This orientation called alignment. After the alignment completes, the NMV increases with the value of the larger alignment, whether positive (parallel alignment- spin up) or negative (antiparallel alignment- spin down) Figure 2.3. At thermal equilibrium, the spin-up are greater than spin-down, thus the NMV directs with $B_0$ direction. This relationship follows the Equation 2.1 (Westbrook *et al*., 2011). The difference between spins gives the magnitude of the NMV and this value depends on the $B_0$.

$$\frac{N^+}{N^-} = e^{-(\Delta E/kT)} \qquad 2.1$$

Where $N^+$ and $N^-$ are the number of spins-up and spins-down populations, respectively; $\Delta E$ is the energy difference between the spin-up and spin-down populations in Joules (J); k is Boltzmann's constant (is the proportionality factor that relates the average relative kinetic energy of particles in a gas with the thermodynamic

temperature of the gas equals to $1.381*10^{-23}$ J/K); and T is the temperature of the tissue in Kelvin (K).

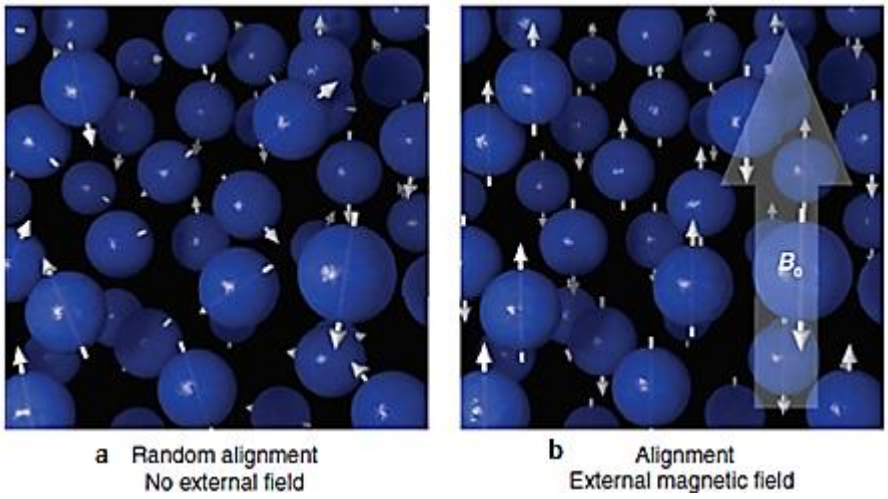


Figure 2. 3: Nuclei alignment. (a): random orientation before allied $B_0$; (b): alignment after $B_0$ applied (Hashemi *et al*., 2012).

After the spin (nuclei motion around own axis) inters $B_0$, it orientes in new motion called precession. The motion speed of the precession (the cycle rotates per second) called processional frequency or Larmor frequency ($\omega_0$) and it measures in megahertz (MHz). The $\omega_0$ estimates by Equation 2.2 and Equation 2.3 (Horowitz, 1992).

$$\Omega_0 = \gamma B_0/2\pi \qquad 2.2$$

simplified to

$$\omega_0 = \gamma B_0 \qquad 2.3$$

Where $\omega_0$ is the precession or Larmor frequency (MHz); $\gamma$ is the gyromagnetic ratio (MHz/T); $B_0$ is the strength of the external magnetic field (Tesla, T). The $2\pi$ function enables the conversion of $\omega_0$ from angular to circular frequency. As $\gamma$ is a constant, for a given MR-active nucleus $\omega_0$ is proportional to $B_0$.

The relationship between angular momentum and the magnetic moment of each MR-active nucleus is called gyromagnetic ratio (γ). The γ is constant with respecting type of nuclei. The γ unit is MHz/T. The highest value of γ is found in $^{1}$H and is equally to 42.58 MHz/T. Other γ of different nuclei presents in Table 2.1.

Table 2.1:The gyromagnetic ration and Larmor frequency of common elements (Westbrook *et al*., 2011).

| **Type of element** | **Gyromagnetic ratio (MHz/T)** | **Larmor frequency at 1.5 T (MHz)** |
|---|---|---|
| **$^{1}$H** | 42.5774 | 63.8646 |
| **$^{13}$C** | 10.7084 | 16.0621 |
| **$^{15}$ N** | 4.3173 | 6.4759 |
| **$^{17}$O** | 5.7743 | 8.6614 |

### 2.3.2 Signal Detection: Relaxation and Reconstruction

To measure the NMV of the hydrogen spins, the spins must move from the external magnetic direction to different direction. The transition occurs by radio-frequency (RF) called RF excitation pulse. Once RF equals to $\omega_0$, the NMV moves from z-direction (suppose the $B_0$ direction in Z direction or longitudinal direction) to xy-direction (transverse direction). Spins are considered to be in the lower energy state when they are rotated with the external magnetic field after that the transition occurs because the energy from RF transfers to spins and the results spin changing own direction to transverse direction, in this stage, the spins are considered to be in the higher energy state. This process is called resonance (Lavdas *et al*., 2013). The result of resonance is transferring the spins from z-axis to xy-axis with spiral motion

(Westbrook *et al*., 2011). All of the spin movement in-phase or coherent magnetization processes in the transverse plane.

When the spins move from the longitudinal axis to the transverse axis, this indicates the flip angle is equal to $90^{\circ}$.The flip angle can change depending on the sequence used in the imaging. Once the spins reach to xy-axis, the signal is created by applying the Faraday's law. Regarding to Faraday's law, the change in magnetic field strength generates an electric current when it passes through a wire (coil). This electric current is caused by the movement of electrons in the magnetic field receiver wire. The electric current turns into a voltage when passes through a resistance. The voltage is called the signal intensity.

The signal intensity received in the coil depends on the frequency of rotation of the magnetic field. Equation 2.4 (Kuo & Wieman, 2016) shows the amount of induced current in a coil is related to the rate of change of magnetic flux.

$$\varepsilon = {}^{-\mathrm{N}\mathrm{d}\varphi}/_{\mathrm{dt}} \qquad 2.4$$

Where ε is the emf in volts (V); N is the number of turns in a coil; d$\varphi$ is changing magnetic flux in a single loop (V/s); and dt is changing time (sec).

The spins return to original alignment -to the $B_0$ – after the RF switched off. The time needs to retain the spins to the initial state called recovery time or $T_1$, and this time is responded for longitudinal relaxation. $T_1$ starts increasing after RF switched off until reaches to the saturation state (all of spins retained to the longitudinal axis). However, the transverse signal starts decreasing (dephasing) due to free induction decay (FID) phenomenon. The time that the spins need to return to normal state in the transverse axis is called decaying time or $T_2$. The $T_1$ time is caused by the

spin loss of energy with the surrounding environment and it is called spin-lattice relaxation. While the loss of energy occurs at $T_1$ time as a result of spin loss of energy with the spin around and it is called spin-spin relaxation. Once the signal is recorded, an inverse Fourier transform is used to reconstruct the image or rotate the M (x, y) distribution. Fourier transform depends on transformation output of the image in frequency domain, while the input image is the spatial domain equivalent. In the Fourier domain image, each point represents a particular frequency contained in the spatial domain image. Discrete Fourier Transform is the sampled Fourier transform and thus does not contain all of the frequencies that make up an image, but only a set of samples large enough to fully describe the spatial field image. The number of frequencies corresponds to the number of pixels in the spatial field image, that is, the image in the spatial domain and the Fourier field has the same size (Park *et al*., 2020).

### 2.3.3 Imaging Properties

The importance of clinical imaging lies in distinguishing between normal tissues and different pathologies. If there is no contrast differentiation between these tissues, it is difficult to distinguish between abnormalities within the body. Comparing MRI with other medical modalities, MRI has the best accuracy to distinguish between soft tissue discrimination, where the sensitivity of MRI is reached to 0.6 and specificity is reached to 0.95 comparing with PET and CT which are estimated to 0.56 in the sensitivity and 0.92 in specificity, and 0.4 in sensitivity and 0.92 in specificity in PET and CT, respectively (Crozier *et al*., 2019). The reason for this distinction is the presence of intrinsic factors in the human body that improves the contrast between tissues and external factors that controlled by the operator (Hashemi *et al*., 2012).

### 2.3.3(a) Signal Intensity of $T_1$

$T_1$ relaxation time, longitudinal relaxation or spin-lattice relaxation occurs after excitation pulse removal through losing the energy from hydrogen spin to the environment medium. The energy losing needs time to occur; thus, the spin-lattice relaxation needs more time than spin-spin relaxation. Indeed, $T_1$ recovery takes 5-10 times more than $T_2$ decay time. Through longitudinal relaxation process, the NMV increasing gradually begins with the loss of energy in the surrounding environment. Therefore, the relaxation depends on type of tissue in the environment medium (Horowitz, 1992).

Spins lose energy dramatically at the start of recovery time. Over the time, the energy loses more slowly until it reaches the full recovery. $T_1$ recovery is the time that longitudinal magnetization reaches to 63% from the original relaxation. $T_1$ recovery can be estimated using Equation 2.5 and Equation 2.6 (Hashemi *et al*., 2012).

$$\mathrm{Mz_t} = \mathrm{M_0}\left(1 - \mathrm{e}^{-\mathrm{t}/T_1}\right) \qquad 2.5$$

$$\mathrm{SI} = \left(1 - \mathrm{e}^{-\mathrm{t}/T_1}\right) \qquad 2.6$$

Where $Mz_t$ is the amount of longitudinal magnetization at time t (millisecond, ms) after the removal of the excitation pulse; $M_0$ is full longitudinal magnetization; $T_1$ is the $T_1$ recovery time (ms) and is the time taken to increase the longitudinal magnetization by a factor of exponential.; and SI is the signal intensity in a tissue. The time (t) in rephasing needs between an RF excitation pulse and next RF excitation pulse is called repetition time (TR).

### 2.3.3(b) Signal Intensity of $T_2$

$T_2$ decay, transverse magnetization, or spin-spin relaxation is obtained by losing the energy from one hydrogen spin to other. The cause of the $T_2$ decay time is the magnetic moments dephasing. In this time the spins coherence are loose (Dale *et al*., 2015).

Despite spin–spin interaction occurs in the same tissue; the dephasing still occurs due to the inhomogeneity in the external magnetic field. Because the $\omega_0$ is proportional depending on $B_0$, the areas which have high magnetic field within the external magnetic field have higher $\omega_0$ (spin slow up). In the same time, the areas which have low inhomogeneity have lower $\omega_0$ (spin slow down). After excitation pulse removes, and due to the inhomogeneity in the magnet field the signal losing faster. This signal is called FID or $T_2^*$signal.

$T_2$ relaxation time depends on the tissue type as well as $T_1$ recovery time. The coherence in the transverse magnetization is high in its early stages and then begins to drop down until all the magnetic moments diphase. $T_2$ decaying has an exponential relationship, and it define the time which reaches to 63% of dephasing at transverse magnetization. $T_2$ decaying time can be estimated using Equation 2.7 and Equation 2.8 (Hashemi *et al*., 2012).

$$\mathrm{Mxy_t} = \mathrm{M_0 e}^{-\mathrm{t}/T_2} \qquad 2.7$$

$$\mathrm{Mxy_t} = \mathrm{M_0 e}^{-\mathrm{t}/\mathrm{T_2^*}} \cos \omega_0 \mathrm{t} \qquad 2.8$$

Where $Mxy_t$ is the amount of transverse magnetization at time t (ms) after the removal of the excitation pulse; $M_0$ is full longitudinal magnetization; $T_2$ is the $T_2$

decay time (ms); $T_2^*$ is relaxation time (ms); and $cos\,\omega_0 t$ is an oscillating wave, with a frequency of $\omega_0$.

The time(t) in dephasing needs between an RF excitation pulse and when signal collected in the receiver coil is called echo time (TE). However, the dephasing caused by inhomogeneities in the $B_0$ field or $T_2^*$ can calculated from Equation 2.9 (Hashemi *et al*., 2012).

$$1/T_2^* = 1/T_2 + 1/2\gamma\Delta B_0 \qquad 2.9$$

Where $T_2$ and $T_2^*$ are the tissues $T_2$ and $T_2^*$ relaxation times (ms); $\gamma$ is the gyromagnetic ratio (MHz/T); and $\Delta B_0$ is the variation in magnetic field (parts per million, ppm). The above equation illustrates the relationship between $T_2$ and $T_2^*$. Therefore, the more inhomogeneities in magnetic field $T_2^*$ being much shorter than $T_2$, and the faster the decaying signal.

## 2.4 MRI Acquisition Sequences

MRI protocols are a group of different MRI sequences. These sequences depend on the type of organ to be imaged and the type of disease to be diagnosed. These sequences differ according to control methods of the pulse, either RF or in the gradient. The difference lies in the way of spin rephasing after excitation pulse. There are two methods to do the rephasing; using 180° RF (spin-echo pulse sequences) or using the gradients (gradient-echo pulse sequences).

There are many different pulse sequences, each has its specific function. Each manufacturer gives a name to these sequences to distinguish between them. Table 2.2 provides a summary of the name of each sequence related to the manufacturer. Among the sequences listed in Table 2.2. $T_2$ HASTE and $T_2$ fat-saturated, Incoherent gradient-

echo $T_1$ in-phase and out-of-phase, and Echo-planar imaging (EPI) are used in liver imaging as routine sequences.

Table 2.2: A comparison of acronyms sequences used by manufacturers (Catherine Westbrook & Talbot, 2018).

| Generic | Siemens | GE | Philips | Hitachi | Toshiba |
|---|---|---|---|---|---|
| **Conventional spin-echo (SE)** | SE | SE | SE | SE | SE |
| **Turbo spin-echo (TSE)** | TSE | FSE | TSE | FSE | FSE |
| **Single-shot TSE (SS-TSE)** | HASTE | SS-FSE | SS-TSE | SS-FSE | FASE |
| **TSE (with restoration pulse)** | RESTORE | FRFSE | DRIVE | Driven equilibrium FSE | $T_2$ Pulse FSE |
| **Inversion recovery (IR)** | IR | IR/MPIR | IR | IR | IR |
| **Fast inversion recovery** | TIR | Fast IR | IR-TSE | IR | IR |
| **Short tau IR (STIR)** | STIR | STIR | STIR | STIR | fast STIR |
| **Fluid-attenuated IR (FLAIR)** | turbo dark fluid | FLAIR | FLAIR | FLAIR | FLAIR |
| **Gradient-echo (GRE)** | GRE | GRE | FFE | GE | field echo |
| **Coherent gradient-echo** | FISP | GRASS | FFE | Rephased SARGE | SSFP |
| **Incoherent gradient-echo** | FLASH | SPGR | $T_1$FFE | spoiled SARGE | fast FE |
| **Reverse-echo gradient-echo** | PSIF | SSFP | $T_2$ FFE | time-reversed SARGE | — |
| **Balanced gradient-echo** | true FISP | FIESTA | BFFE | balanced SARGE | true SSFP |
| **Echo-planar imaging (EPI)** | EPI | EPI | EPI | EPI | EPI |
| **Double-echo steady state** | DESS | — | — | — | — |
| **Balanced dual excitation** | CISS | FIESTA-C | — | phase balanced SARGE | — |
| **Multi-echo-data-image-combination** | MEDIC | MERGE | MFFE | — | — |
| **Fast gradient-echo** | turbo FLASH | fast GRE, fast SPGR | TFE | RGE | Fast FE |
| **Hybrid sequence** | TGSE | — | GRASE | — | Hybrid EPI |

### 2.4.1 Single-Shot TSE (HASTE)

Half-Fourier acquisition single-shot turbo spin-echo (HASTE) is one of the single-shot forms used to reduce the time during one TR. The information (signal obtained from organ and save as a digital information) in this form is filled to more than one line in k-space in the same one TR. It is called single-shot because all lines in k-space are filled once. It obtains all the information during single echo train (Schulz *et al*., 2018).

To achieve single-shot, multi-echoes propagate with different phase encoding using different gradient slope to fill all the lines in k-space in a single-shot. The rapid movement of phase-encoding gradient allows changing the direction of filling in the k-space. Because applying the short time in the single-shot, it uses with combination $T_2$ contrast imaging at different clinical practices (Mulkern *et al*., 1990; Leitão *et al*., 2013). Due to very short acquisition time and greater resistance to susceptibility and motion artefacts, this technique is used for scout images, children cases, uncooperative patients, non-breath-hold abdominal imaging, and fetal imaging. HASTE sequence used high number of 180° to obtain the multi-echoes in a short time and thus the susceptibility decreases because of decreased time for dephasing between 180-degree pulses (Guglielmo *et al*., 2014). Therefore, the refocusing pulses are used with applying high RF. Indeed, this technique affects spatial resolution through HASTE sequence with a continuous slice acquisition will have a high SNR in the first image followed by low SNR in subsequent images (Henzler *et al*., 2009).

Donato *et al*. (2017) reported the benefit of HASTE sequences in liver imaging, because the HASTE sequence reduces the motion artifact which is high due to the breathing movement. If there is two breath-holds are required, it needs a sequential

acquisition to perform and avoid misregistration artefacts and this can be done using HASTE.

### 2.4.2 Incoherent Gradient-Echo (FLASH)

Very fast sequences should be used for the volume case in a single breath hold. One of these sequences is incoherent gradient-echo. Incoherent gradient echo uses extremely short TR and short TE to suppress susceptibility artifacts. This sequence uses a small part of the RF through the application of a small flip angle. Thus, the sequence takes less time to apply RF and switch off. However, partial echo will be received in the coil. This technique is used when the temporal resolution is required. Indeed, this technique is very essential after administration of contrast agent (CA) during the dynamic imaging. Because the TR and the flip angle are very short, incoherent gradient-echo improves $T_1$ contrast. TR times as brief as 20 to 30 ms while retaining reasonable signal levels (Westbrook & Talbot, 2018).

Fast low-angle shot (FLASH) or spoiled gradient recalled echo (SPGR) is a steady- state saturation recovery gradient echo sequence uses this technique; it has several benefits: it can be used to manipulate the differences from varying intrinsic tissue parameters; and it is very fast MR sequence.

For this sequence, the signal intensity is measured by solving steady-state Bloch equation 2.10 (Fischl *et al*., 2004) as the following:

$$\mathrm{SI} = \mathrm{k[H]}\frac{\sin\theta\left(1-\mathrm{e}^{-\mathrm{TR}/T_1}\right)}{1-\cos\theta\,\mathrm{e}^{-\mathrm{TR}/T_1}}\,\mathrm{e}^{-\mathrm{TE}/T_2{}^*} \qquad 2.10$$

Where k is a scaling factor; TR is the repetition time (ms); $T_1$ is the $T_1$ relaxation time of a tissue (ms); $TE$ is the echo time (ms); $T_2^*$ is relaxation time (ms); and $\theta$ is the flip angle.

Through the short flip angle in steady state sequence, the optimum flip angle is determined by the Ernst angle equation (Equation 2.11) (Horowitz, 1992) which provides the highest signal intensity for tissue with given TR.

$$\text{Ernst} = \cos^{-1} e^{-\text{TR}/T_1} \quad 2.11$$

Where Ernst is the Ernst angle in degrees; TR is the repetition time (ms); and $T_1$ is the $T_1$ relaxation time of a tissue (ms). This equation determines the maximum signal intensity for a tissue with a certain $T_1$ relaxation time at different TR values. When the flip angle is larger than the Ernst angle, saturation will happen and therefore $T_1$ contrast increases. When the flip angle is less than the Ernst angle, contrast relies more on proton density (PD).

The steady state includes very short TR with repeated RF excitation pulse. Because TR is very short in $T_1$ (TR = 4-6 ms, TE = 1-3 ms, flip angle = 10º-15º), the residual transverse magnetisation is built up. The residual transverse magnetization is recovered by RF excitation pulse usually have a magnitude of 90° and rephasing pulse magnitude of 180°.

Jajamovich *et al*. (2016) reported the benefit of FLASH sequences in liver imaging to detect the quantification of HCC through combination of this sequence with direct contrast enhancement (DCE) sequence. They showed that FLASH should be used as routine sequence in liver MR imaging. Another study by the researcher Getzin *et al*. (2018) evaluated the Gd-EOB-DTPA-enhanced MRI for assessment liver organ damage after the injury of hepatic ischemia. The study conducted in mice and found the FLASH sequence and other sequences can be applied in the future studies to assess the liver damage.